ELSEVIER

Engineering Analysis with Boundary Elements 25 (2001) 639–653

ENGINEERING ANALYSIS *with* BOUNDARY ELEMENTS

www.elsevier.com/locate/enganabound

The meshless hypersingular boundary node method for three-dimensional potential theory and linear elasticity problems

Mandar K. Chati[a,1], Subrata Mukherjee[a,*], Glaucio H. Paulino[b]

[a]*Department of Theoretical and Applied Mechanics, Kimball Hall, Cornell University, Ithaca, NY 14853-1503, USA*
[b]*Department of Civil and Environmental Engineering, University of Illinois, Newmark Laboratory, 205 N. Mathews Avenue, Urbana, IL 61801, USA*

Received 23 August 2000; accepted 25 January 2001

Abstract

The Boundary Node Method (BNM) represents a coupling between Boundary Integral Equations (BIEs) and Moving Least Squares (MLS) approximants. The main idea here is to retain the dimensionality advantage of the former and the meshless attribute of the latter. The result is a 'meshfree' method that decouples the mesh and the interpolation procedures. The BNM has been applied to solve 2-D and 3-D problems in potential theory and linear elasticity. The Hypersingular Boundary Element Method (HBEM) has diverse important applications in areas such as fracture mechanics, wave scattering, error analysis and adaptivity, and to obtain a symmetric Galerkin boundary element formulation. The present work presents a coupling of Hypersingular Boundary Integral Equations (HBIEs) with MLS approximants, to produce a new meshfree method — the Hypersingular Boundary Node Method (HBNM). Numerical results from this new method, for selected 3-D problems in potential theory and in linear elasticity, are presented and discussed in this paper.

Keywords: Boundary element method; Boundary mode method; Hypersingular integrals; Potential theory; Linear elasticity

1. Introduction

Conventional computational engines such as the Finite Difference Method (FDM), Finite Element Method (FEM), and the Boundary Element Method (BEM) require meshing of either the domain (FEM and FDM) or the surface (BEM) of a solid body. Although significant progress has been made in 3-D meshing algorithms (see Mackerle [1]), the task of meshing a 3-D object with complicated geometry can be arduous, time consuming, computationally cumbersome and expensive. Such shortcomings are greatly amplified when one considers problems with changing geometry such as crack propagation, finite deformation, and phase change or shape optimization. The main difficulty in these problems is the task of re-meshing a 3-D object many times during a solution process.

1.1. Meshfree methods

In recent years, novel computational algorithms have been proposed that circumvent some of the problems associated with 3-D meshing. These methods have been collectively referred to as 'meshfree' or 'meshless' methods. Nayroles et al. [2] proposed a method called the Diffuse Element Method (DEM). The main idea of their work is to replace the usual FEM interpolation by a 'diffuse approximation'. Their strategy consists of using a moving least-squares approximation scheme to interpolate the field variables — these are called MLS interpolants in Ref. [2] (called MLS approximants in this work). Nayroles et al. [2] have applied the DEM to 2-D problems in potential theory and linear elasticity.

Meshfree methods proposed to date include the Element-Free Galerkin (EFG) method (Belytschko et al. [3]), the Reproducing Kernel Particle Method (RKPM) [4], h–p clouds [5–7], the Meshless Local Petrov-Galerkin (MLPG) approach [8,9], the Local Boundary Integral Equation (LBIE) method [10], the Natural Element Method (NEM) [11], the Generalized Finite Element Method (GFEM) [12] — see Moës et al. [13] for related work) and the Boundary Node Method (BNM). The main idea in the EFG method is to use Moving Least Squares (MLS) approximants to construct the trial functions used in the Galerkin weak form. A wide variety of problems have been solved using the EFG method. In the introductory paper by Belytschko et al. [3], the EFG method was applied

* Corresponding author. Tel.: +1-607-255-7143; fax: +1-607-255-2011.
E-mail address: sm85@cornell.edu (S. Mukherjee).
[1] Present address: General Electric, Corporate Research and Development, Schenectady, NY 12301.

0955-7997/01/$ - see front matter
PII: S0955-7997(01)00040-6

to 2-D problems in linear elasticity and heat conduction. Since then, the method has been applied, for example, to solve problems in elasto-plasticity [14], fracture mechanics [15], crack growth [16,17], dynamic fracture [18,19,20], elasto-plastic fracture mechanics [21,22], plate bending [23], thin shells [24], and sensitivity analysis and shape optimization [25]. A special issue of the journal *Computer Methods in Applied Mechanics and Engineering* contains review articles by Belytschko et al. [26] and Liu et al. [27], in addition to various other research papers on meshless methods. Another source of information on the RKPM is an overview article by Liu et al. [28].

1.2. Hypersingular Boundary Element Method (HBEM)

Hypersingular Boundary Integral Equations (HBIEs) are derived from a differentiated version of the usual boundary integral equations (BIEs). HBIEs have diverse important applications and are the subject of considerable current research (see, for example, [29–32] for recent surveys of the field). HBIEs, for example, have been employed for the evaluation of boundary stresses (e.g. [33–36]), in wave scattering (e.g. [37]), in fracture mechanics (e.g. [31,38–41]), to obtain symmetric Galerkin boundary element formulations (e.g. [42–45]), to obtain the hypersingular boundary contour method [46,47], and for error analysis [48–52] and adaptivity ([51,52]). A lively debate (e.g. [53,54]), on smoothness requirements on boundary variables for collocating an HBIE on the boundary of a body, has apparently been concluded recently [55], see also Ref. [52]).

1.3. BNM

Mukherjee and Mukherjee [56] have recently proposed a meshfree method called the BNM. The BNM has been used for 2-D problems in potential theory [56] and linear elasticity [57], for 3-D problems in potential theory [58] and linear elasticity [59], and for error analysis and adaptivity [51]. This method is a combination of the MLS approximation scheme and the standard BIE method. The method divorces the traditional coupling between spatial discretization (meshing) and interpolation as commonly practiced in the FEM or in the BEM. Instead, a 'diffuse' approximation, based on MLS approximants, is used to represent the unknown functions; and surface cells, with a very flexible structure (e.g. any cell can be arbitrarily subdivided without affecting its neighbors), are used for integration (Fig. 1). Thus, the BNM retains the *meshless attribute of the EFG method and the dimensionality advantage of the BEM*. As a consequence, the BNM only requires the specification of *points on the 2-D bounding surface* of a 3-D body (including crack faces in fracture mechanics problems), together with unstructured surface cells, thereby practically eliminating the meshing problem that has been referred to previously. In contrast, the FEM needs volume meshing, the BEM needs surface meshing, and the EFG needs points throughout the domain of a body.

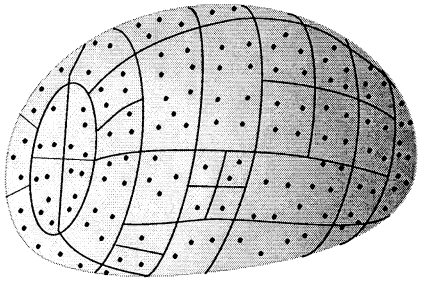

Fig. 1. BNM or HBNM input data structure: cells and collocation nodes.

1.4. Outline of this paper

The HBNM is obtained by combining the HBIE for a given boundary value problem with MLS approximants. The HBNM is derived from the appropriate HBIE, for potential theory and for linear elasticity, and is then numerically implemented in the present paper.

This paper is organized as follows. A brief literature review is provided in this Section. Next, Section 2 presents MLS approximants, including a technique for evaluation of tangential derivatives on the boundary. Section 3 reviews the standard BIE employed in the traditional collocation-based BEM, and Section 4 its corresponding meshless version called the BNM. Section 5 presents the HBIE and Section 6 the HBNM, which is obtained from the corresponding HBIE. Numerical results from the HBNM, for problems in potential theory and in linear elasticity, are presented in Section 7. Several aspects of the HBNM, such as position of collocation nodes, determination of geodesics, range of influence of nodes, solution at internal points, accuracy and convergence properties, are investigated in Section 7. Finally, some concluding remarks are presented in Section 8. Appendix A completes the paper.

2. Surface approximants

A moving least-squares (MLS) approximation scheme, using curvilinear coordinates on the surface of a 3-D solid body, is suitable for the BNM. Such a scheme for problems in potential theory [58] and for linear elasticity [59] is briefly described here and employed in the theoretical and numerical schemes that follow.

2.1. MLS approximants

It is assumed that, for 3-D problems, the bounding surface ∂B of a solid body is the union of piecewise smooth segments called panels. On each panel, one defines surface curvilinear coordinates (s_1, s_2). For 3-D problems in potential theory, let u be the potential function and $\tau \equiv \partial u/\partial n$ the flux. (Here $\mathbf{n}$ is an unit outward normal to ∂B at a point on it). For

3-D linear elasticity, let u denote a component of the displacement vector $\mathbf{u}$ and τ be a component of the traction vector $\boldsymbol{\tau}$ on ∂B. One defines:

$$u(\mathbf{s}) = \sum_{i=1}^{m} p_i(\mathbf{s} - \mathbf{s}^E)a_i = \mathbf{p}^T(\mathbf{s} - \mathbf{s}^E)\mathbf{a},$$
$$\tau(\mathbf{s}) = \sum_{i=1}^{m} p_i(\mathbf{s} - \mathbf{s}^E)b_i = \mathbf{p}^T(\mathbf{s} - \mathbf{s}^E)\mathbf{b}. \tag{1}$$

The monomials p_i (see below) are evaluated in local coordinates $(s_1 - s_1^E, s_2 - s_2^E)$, where (s_1^E, s_2^E) are the global coordinates of an evaluation point E. It is important to state here that a_i and b_i are not constants. Their functional dependencies are determined later. The name 'MLS' arises from the fact that the quantities a_i and b_i are not constants. The integer m is the number of monomials in the basis used for u and τ. Quadratic approximants, for example, are of the form:

$$\mathbf{p}^T(\tilde{s}_1, \tilde{s}_2) = [1, \tilde{s}_1, \tilde{s}_2, \tilde{s}_1^2, \tilde{s}_2^2, \tilde{s}_1\tilde{s}_2],$$
$$m = 6, \quad \tilde{s}_i = s_i - s_i^E; \quad i = 1, 2. \tag{2}$$

The coefficients a_i, and b_i are obtained by minimizing the weighted discrete L_2 norms:

$$R_u = \sum_{I=1}^{n} w_I(d)[\mathbf{p}^T(\mathbf{s}^I - \mathbf{s}^E)\mathbf{a} - \hat{u}_I]^2,$$
$$R_\tau = \sum_{I=1}^{n} w_I(d)[\mathbf{p}^T(\mathbf{s}^I - \mathbf{s}^E)\mathbf{b} - \hat{\tau}_I]^2, \tag{3}$$

where the summation is carried out over the n boundary nodes for which the weight function satisfies the inequality $w_I(d) \neq 0$. (Weight functions are defined in Section 2.3). The quantity $d = g(\mathbf{s}, \mathbf{s}_I)$ is the length of the geodesic on ∂B between $\mathbf{s}$ and $\mathbf{s}^I$. These n nodes are said to be within the domain of dependence of a point $\mathbf{s}$ (evaluation point E in Fig. 2(a)). Also, $(s_1^I - s_1^E, s_2^I - s_2^E)$ are the local surface coordinates of the boundary nodes with respect to the evaluation points $\mathbf{s}^E = (s_1^E, s_2^E)$ and $\hat{u}_I$ and $\hat{\tau}_I$ are the approximations to the nodal values u_I and τ_I. These equations above can be rewritten in compact form as:

$$R_u = (\mathbf{P}(\mathbf{s}^I - \mathbf{s}^E)\mathbf{a} - \hat{\boldsymbol{u}})^T\mathbf{W}(\mathbf{s}, \mathbf{s}^I)(\mathbf{P}(\mathbf{s}^I - \mathbf{s}^E)\mathbf{a} - \hat{\boldsymbol{u}}), \tag{4}$$

$$R_\tau = (\mathbf{P}(\mathbf{s}^I - \mathbf{s}^E)\mathbf{b} - \hat{\boldsymbol{\tau}})^T\mathbf{W}(\mathbf{s}, \mathbf{s}^I)(\mathbf{P}(\mathbf{s}^I - \mathbf{s}^E)\mathbf{b} - \hat{\boldsymbol{\tau}}), \tag{5}$$

where $\hat{\boldsymbol{u}}^T = (\hat{u}_1, \hat{u}_2, \ldots, \hat{u}_n)$, $\hat{\boldsymbol{\tau}}^T = (\hat{\tau}_1, \hat{\tau}_2, \ldots, \hat{\tau}_n)$, $\mathbf{P}(\mathbf{s}^I)$ is an $n \times m$ matrix whose kth row is:

$$[1, p_2(s_1^k, s_2^k), \ldots, p_m(s_1^k, s_2^k)]$$

and $\mathbf{W}(\mathbf{s},\mathbf{s}^I)$ is an $n \times n$ diagonal matrix with $w_{kk} = w_k(d)$ (no sum over k). A typical weight function $w_I(d)$ is shown in Fig. 2(b) and is discussed in Section 2.3.

The stationarity of R_u and R_τ, with respect to $\mathbf{a}$ and $\mathbf{b}$, respectively, leads to the equations:

$$\mathbf{a}(\mathbf{s}) = \mathbf{A}^{-1}(\mathbf{s})\mathbf{B}(\mathbf{s})\hat{\boldsymbol{u}}, \qquad \mathbf{b}(\mathbf{s}) = \mathbf{A}^{-1}(\mathbf{s})\mathbf{B}(\mathbf{s})\hat{\boldsymbol{\tau}}, \tag{6}$$

where

$$\mathbf{A}(\mathbf{s}) = \mathbf{P}^T(\mathbf{s}^I - \mathbf{s}^E)\mathbf{W}(\mathbf{s}, \mathbf{s}^I)\mathbf{P}(\mathbf{s}^I - \mathbf{s}^E),$$
$$\mathbf{B}(\mathbf{s}) = \mathbf{P}^T(\mathbf{s}^I - \mathbf{s}^E)\mathbf{W}(\mathbf{s}, \mathbf{s}^I). \tag{7}$$

It is noted from above that the coefficients a_i and b_i turn out to be functions of $\mathbf{s}$.

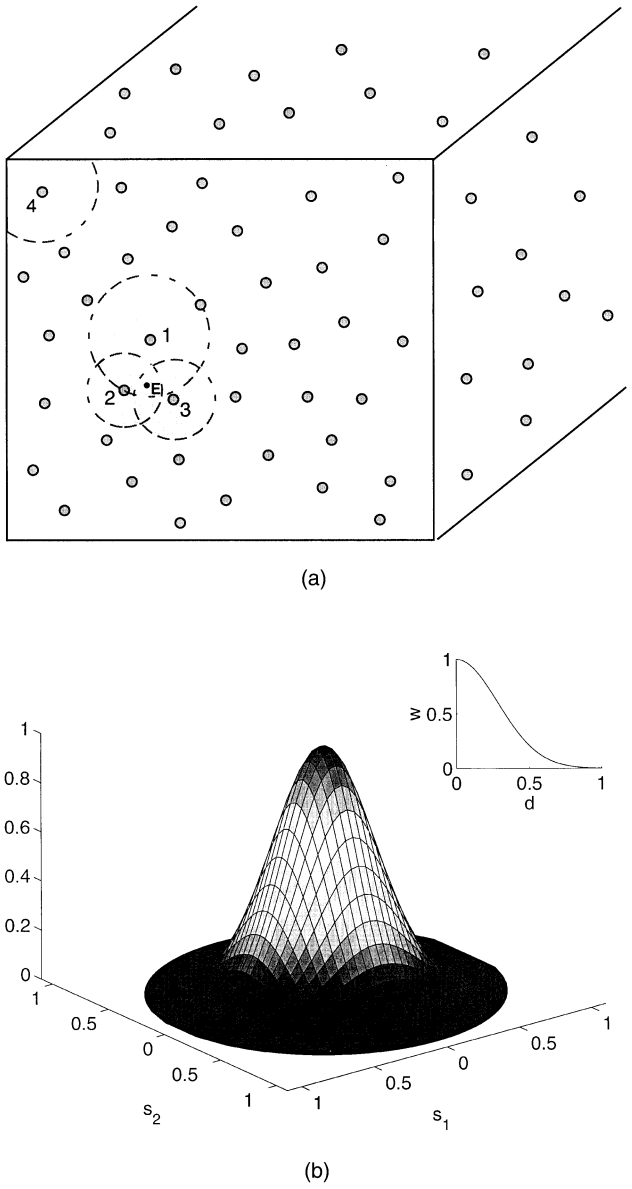

Fig. 2. Domain of dependence and range of influence. (a) The nodes 1, 2 and 3 lie within the domain of dependence of the evaluation point E. The ranges of influence of nodes 1, 2, 3 and 4 are shown as gray circles. The range of influence of node 4 is truncated at the edges of the body. (b) Gaussian weight function defined on the range of influence of a node.

Substitution of Eq. (6) into Eq. (1) leads to:

$$u(\mathbf{s}) = \sum_{I=1}^{n} \Phi_I(\mathbf{s})\hat{u}_I, \qquad \tau(\mathbf{s}) = \sum_{I=1}^{n} \Phi_I(\mathbf{s})\hat{\tau}_I, \tag{8}$$

where the approximating functions are Φ_I are:

$$\Phi_I(\mathbf{s}) = \sum_{j=1}^{m} p_j(\mathbf{s} - \mathbf{s}^E)(\mathbf{A}^{-1}\mathbf{B})_{jI}(\mathbf{s}). \tag{9}$$

As mentioned previously, $\hat{u}$ and $\hat{\tau}$ are approximations to the actual nodal values u and τ. The two sets of values are related by Eq. (8). Discretized versions of Eq. (8) can be written as:

$$[\mathbf{H}]\{\hat{u}_k\} = \{u_k\}, \qquad [\mathbf{H}]\{\hat{\tau}_k\} = \{\tau_k\}, \qquad k = 1, 2, 3. \tag{10}$$

Eq. (10) relate the nodal approximations of u and τ to their nodal values.

2.2. Surface derivatives

Surface derivatives of the potential (or displacement) field u are required for the HBIE. These are computed as follows. With

$$\mathbf{C} = \mathbf{A}^{-1}\mathbf{B}$$

Eqs. (8) and (9) give:

$$u(\mathbf{s}) = \sum_{I=1}^{n}\sum_{j=1}^{m} p_j(\mathbf{s} - \mathbf{s}^E)\mathrm{C}_{jI}(\mathbf{s})\hat{u}_I \tag{11}$$

and the tangential derivatives of u can be written as:

$$\frac{\partial u(\mathbf{s})}{\partial s_k} = \sum_{I=1}^{n}\sum_{j=1}^{m}\left[\frac{\partial p_j}{\partial s_k}(\mathbf{s} - \mathbf{s}^E)\mathrm{C}_{jI}(\mathbf{s}) + p_j(\mathbf{s} - \mathbf{s}^E)\frac{\partial C_{jI}(\mathbf{s})}{\partial s_k}\right]\hat{u}_I$$

$$k = 1, 2. \tag{12}$$

The derivatives of the monomials p_j can be promptly computed. These are:

$$\frac{\partial \mathbf{p}^T}{\partial s_1}(s_1 - s_1^E, s_2 - s_2^E) = [0, 1, 0, 2(s_1 - s_1^E), 0, (s_2 - s_2^E)], \tag{13}$$

$$\frac{\partial \mathbf{p}^T}{\partial s_2}(s_1 - s_1^E, s_2 - s_2^E) = [0, 0, 1, 0, 2(s_2 - s_2^E), (s_1 - s_1^E)]. \tag{14}$$

After some simple algebra (Chati [60]), the derivatives of the matrix $\mathbf{C}$ with respect to s_k take the form:

$$\frac{\partial \mathbf{C}(\mathbf{s})}{\partial s_k} = -\mathbf{A}^{-1}(\mathbf{s})\frac{\partial \mathbf{B}(\mathbf{s})}{\partial s_k}\mathbf{P}(\mathbf{s}^I - \mathbf{s}^E)\mathbf{A}^{-1}(\mathbf{s})\mathbf{B}(\mathbf{s}) + \mathbf{A}^{-1}(\mathbf{s})\frac{\partial \mathbf{B}(\mathbf{s})}{\partial s_k}, \qquad k = 1, 2, \tag{15}$$

with

$$\frac{\partial \mathbf{B}(\mathbf{s})}{\partial s_k} = \mathbf{P}^T(\mathbf{s}^I - \mathbf{s}^E)\frac{\partial \mathbf{W}(\mathbf{s},\mathbf{s}^I)}{\partial s_k}. \tag{16}$$

In deriving Eq. (15), the following identity has been used:

$$\frac{\partial \mathbf{A}^{-1}(\mathbf{s})}{\partial s_k} = -\mathbf{A}^{-1}(\mathbf{s})\frac{\partial \mathbf{A}(\mathbf{s})}{\partial s_k}\mathbf{A}^{-1}(\mathbf{s}), \qquad k = 1, 2. \tag{17}$$

Tangential derivatives of the weight functions (described in Section 2.3) are easily computed (Chati [60]). The final form of the tangential derivatives of the potential (or displacement) u, at an evaluation point E, takes the form:

$$\frac{\partial u}{\partial s_k}(\mathbf{s}^E) = \sum_{I=1}^{n}\sum_{j=1}^{m}\left[\frac{\partial p_j}{\partial s_k}(0,0)\mathrm{C}_{jI}(\mathbf{s}^E)\right]\hat{u}_I + \sum_{I=1}^{n}\sum_{j=1}^{m} \times\left[p_j(0,0)\left\{\mathbf{A}^{-1}(\mathbf{s}^E)\frac{\partial \mathbf{B}}{\partial s_k}(\mathbf{s}^E)(\mathbf{I} - \mathbf{P}(\mathbf{s}^I - \mathbf{s}^E) \times \mathbf{A}^{-1}(\mathbf{s}^E)\mathbf{B}(\mathbf{s}^E))\right\}\right]\hat{u}_I \tag{18}$$

with $k = 1, 2$. In the above equation, $\mathbf{I}$ is the identity matrix.

One also needs the spatial gradient of the function u in order to solve the HBIE (see Sections 5 and 6). For problems in potential theory, this is easily obtained from its tangential and normal derivatives $\partial u/\partial s_k$ and $\partial u/\partial n$, respectively. For elasticity problems, however, one must also use Hooke's law at a point on the surface ∂B. Details of this procedure are given in Appendix A.

Eq. (18) can be rewritten in compact form as:

$$\frac{\partial u}{\partial s_k}(\mathbf{s}^E) = \sum_{I=1}^{n} \Psi_I^{(k)}(\mathbf{s}^E)\hat{u}_I; \qquad k = 1, 2, \tag{19}$$

where the approximating functions Ψ_I^k are:

$$\Psi_I^{(k)}(\mathbf{s}^E) = \sum_{j=1}^{m}\left[\frac{\partial p_j}{\partial s_k}(0,0)\mathrm{C}_{jI}(\mathbf{s}^E)\right] + \sum_{j=1}^{m}\left[p_j(0,0)\left\{\mathbf{A}^{-1}(\mathbf{s}^E)\frac{\partial \mathbf{B}}{\partial s_k}(\mathbf{s}^E) \times (\mathbf{I} - \mathbf{P}(\mathbf{s}^I - \mathbf{s}^E)\mathbf{A}^{-1}(\mathbf{s}^E)\mathbf{B}(\mathbf{s}^E))\right\}\right]. \tag{20}$$

2.3. Weight functions

The basic idea behind the choice of a weight function is that its value should decrease with distance from a node and that it should have compact support so that the region of influence of a node is of finite extent (Fig. 2(b)). A possible choice is the Gaussian weight function:

$$w_I(d) = \begin{cases} \mathrm{e}^{-(d/d_I)^2} & \text{for } d \le d_I, \\ 0 & \text{for } d > d_I. \end{cases} \tag{21}$$

Here $d = g(\mathbf{s}, \mathbf{s}^I)$ is the *minimum distance*, measured on the surface ∂B, (i.e. the geodesic) between a point $\mathbf{s}$ and the collocation node I. In the research performed to date, the region of influence of a node has been truncated at the edge of a panel (Fig. 2(a)) so that geodesics, and their derivatives (for use in Eq. (21)), need only be computed on piecewise smooth surfaces. Finally, the quantities d_I determine the extent of the region of influence (the compact support) of node I. They can be made globally uniform, or can be adjusted such that approximately the same number of nodes get included in the region of influence of any given node I or in the domain of dependence of a given evaluation point E. Such ideas have been successfully implemented in Refs. [58,59].

3. BIEs

The standard (singular) BIEs for potential theory and linear elasticity are given below. It is hoped that the sequence of presentations below will help towards a clear understanding of boundary-based meshless methods.

3.1. Potential theory

The well known regularized BIE for 3-D problems in potential theory is (see, for example, Banerjee [61]:

$$0 = \int_{\partial B} [G(P,Q)\tau(Q) - F(P,Q)(u(Q) - u(P))]\, \mathrm{d}S_Q, \quad (22)$$

where, as mentioned before, u is the potential, $\tau = \partial u/\partial n$ is the flux, and the kernels for 3-D problems are:

$$G(P,Q) = \frac{1}{4\pi r(P,Q)}, \qquad F(P,Q) = \frac{\partial G(P,Q)}{\partial n_Q}. \quad (23)$$

Here, r is the Euclidean distance between the source point P and field point Q, and n_Q is the unit normal to ∂B at a (regular) field point Q.

3.2. Linear elasticity

For 3-D linear elasticity, the standard BIE, in regularized form, and in the absence of body forces, can be written as ([62])

$$0 = \int_{\partial B} [U_{ik}(P,Q)\tau_k(Q) - T_{ik}(P,Q)(u_k(Q) - u_k(P))]\, \mathrm{d}S_Q, \quad (24)$$

where u_k and τ_k are the components of the displacement and traction respectively, and the Kelvin kernels are:

$$U_{ik} = \frac{1}{16\pi(1-\nu)Gr}[(3-4\nu)\delta_{ik} + r_{,i}r_{,k}], \quad (25)$$

$$T_{ik} = \frac{-1}{8\pi(1-\nu)r^2}\Bigg[\{(1-2\nu)\delta_{ik} + 3r_{,i}r_{,k}\}\frac{\partial r}{\partial n} - (1-2\nu)(r_{,i}n_k - r_{,k}n_i)\Bigg]. \quad (26)$$

In the above, n_i are the components of the unit normal at the field point Q, G is the shear modulus, ν is the Poisson ratio and δ_{ij} denotes the Kronecker delta. A comma denotes a derivative with respect to a field point, i.e.

$$r_{,i} = \frac{\partial r}{\partial x_i(Q)} = \frac{x_i(Q) - x_i(P)}{r}. \quad (27)$$

4. BNM

The MLS approximates derived in Section 2 are used to approximate u and τ on the boundary ∂B. In order to carry out the integrations, the bounding surface is discretized into cells. A variety of shape functions have been used in order to interpolate the geometry. In particular, the bilinear (Q4) and quadratic (T6) triangle cells have been employed. These 'geometric' shape functions can be found in any standard text on the FEM (see [63,64]).

4.1. Potential theory

Substituting the expressions for u and τ from Eq. (8) into Eq. (22), and dividing ∂B into N_c cells, one gets the discretized form of the BIE for potential problems as follows:

$$0 = \sum_{k=1}^{N_c} \int_{\partial B_k} \Bigg[G(P,Q) \sum_{I=1}^{N_Q} \Phi_I(Q)\hat{\tau}_I - F(P,Q) \times \Bigg\{ \sum_{I=1}^{N_Q} \Phi_I(Q)\hat{u}_I - \sum_{I=1}^{N_P} \Phi_I(P)\hat{u}_I \Bigg\} \Bigg] \mathrm{d}S_Q. \quad (28)$$

where $\Phi_I(P)$ and $\Phi_I(Q)$ are the contributions from the Ith node to the collocation point P and field point Q, respectively. Also, N_Q nodes are situated in the domain of dependence of the field point Q and N_P nodes are situated in the domain of dependence of the source point P.

4.2. Linear elasticity

The BNM equation for elasticity is obtained by substituting the expressions for u_k and τ_k (Eq. (8) into Eq. (24), leading

to:

$$0 = \sum_{m=1}^{N_c} \int_{\partial B_m} \left[U_{ik}(P,Q) \sum_{I=1}^{N_Q} \Phi_I(Q) \hat{\tau}_{kI} - T_{ik}(P,Q) \times \left\{ \sum_{I=1}^{N_Q} \Phi_I(Q) \hat{u}_{kI} - \sum_{I=1}^{N_P} \Phi_I(P) \hat{u}_{kI} \right\} \right] \mathrm{d}S_Q. \quad (29)$$

4.3. Discretization

In order to evaluate the non-singular integrals in Eqs. (28) and (29) over (possibly curved) triangular or rectangular surface cells, 7 point and 3×3 Gauss quadrature are used, respectively. However, as $Q \to P$ the kernels G and U_{ik} become weakly singular and the kernels F and T_{ik} become strongly singular. As shown in Eqs. (28) and (29), the strongly singular integrands are regularized by using rigid body modes and the regularized versions are weakly singular. Finally, special integration techniques are used to evaluate the resulting weakly singular integrals in Eqs. (28) and (29) ([58,65]).

The final discretized version of either Eq. (28) or Eq. (29) has the form:

$$[\mathbf{A}_{(\hat{u})}]\{\hat{\mathbf{u}}\} + [\mathbf{A}_{(\hat{\tau})}]\{\hat{\boldsymbol{\tau}}\} = \{0\}. \quad (30)$$

With respect to elasticity theory, the count for the number of equations and unknowns follows. For N_B nodes on the bounding surface, there are a total of $12N_B$ quantities on the boundary, i.e. $3N_B$ values for each of u_i and its nodal approximation $\hat{u}_i$, and similarly for τ_i. For a well posed problem, values of either u_i or τ_i are known at each node on the boundary, so $3N_B$ nodal values are given. Therefore, $9N_B$ equations are needed to solve for the $9N_B$ remaining unknowns. Eq. (30) consists of $3N_B$ equations and Eq. (10) consist of $3N_B$ equations each. Thus, a well-posed boundary value problem can be solved using Eq. (30), in combination with Eq. (20). An analogous count of equations and unknowns applies to Eq. (28) for potential theory.

5. HBIEs

Continuing the basic development of Section 3, the HBIEs for potential theory and linear elasticity are presented here.

5.1. Potential theory

The HBIE is obtained upon differentiation of the primary BIE at an internal source point with respect to the coordinates of that source point. Due to differentiation, the kernels in the HBIE become strongly singular and hypersingular, respectively, and appropriate regularization procedures need to be employed in order to use the HBIEs for carrying out meaningful computations. The fully regularized HBIE for the Laplace's equation, at a regular point on ∂B (where it is locally smooth) can be written as (see Krishnasamy et al. [29]),

$$0 = \int_{\partial B} \frac{\partial G(P,Q)}{\partial x_m(P)} [\tau(Q) - \tau(P)] \, \mathrm{d}S_Q - u_{,k}(P) \int_{\partial B} \frac{\partial G(P,Q)}{\partial x_m(P)} [n_k(Q) - n_k(P)) \, \mathrm{d}S_Q - \int_{\partial B} \frac{\partial F(P,Q)}{\partial x_m(P)} [u(Q) - u(P) - u_{,k}(P)(x_k(\mathrm{Q}) - x_k(P))] \mathrm{d}S_Q. \quad (31)$$

Carrying out the inner product of Eq. (31) with the source point normal $\mathbf{n}(P)$, one obtains:

$$0 = \int_{\partial B} \frac{\partial G(P,Q)}{\partial n(P)} [\tau(Q) - \tau(P)] \, \mathrm{d}S_Q - u_{,k}(P) \int_{\partial B} \frac{\partial G(P,Q)}{\partial n(P)} (n_k(Q) - n_k(P)) \, \mathrm{d}S_Q - \int_{\partial B} \frac{\partial F(P,Q)}{\partial n(P)} [u(Q) - u(P) - u_{,k}(P)(x_k(Q) - x_k(P))] \, \mathrm{d}S_Q. \quad (32)$$

The gradient of the potential function is required in the HBIEs Eqs. (31) and (32). For potential problems, the gradient (at a regular boundary point) can be written as,

$$\nabla u = \frac{\partial u}{\partial s_1} \mathbf{t}_1 + \frac{\partial u}{\partial s_2} \mathbf{t}_2 + \tau \, \mathbf{n}, \quad (33)$$

where $\tau = \partial u / \partial n$ is the flux, $\mathbf{n}$ is the unit normal, $\mathbf{t}_1$, $\mathbf{t}_2$ are the appropriately chosen unit vectors in two tangential directions on the surface of the body, and $\partial u / \partial s_i$, $i = 1, 2$ are the tangential derivatives of u (along $\mathbf{t}_1$ and $\mathbf{t}_2$) on the surface of the body.

5.2. Linear elasticity

Similarly, the fully regularized HBIE for linear elasticity can be written as (see Cruse and Richardson [54]),

$$0 = \int_{\partial B} D_{ijk}(P,Q)(\tau_k(Q) - \tau_k(P)) \, \mathrm{d}S_Q - \sigma_{km}(P) \int_{\partial B} D_{ijk}(P,Q)(n_m(Q) - n_m(P)) \, \mathrm{d}S_Q - \int_{\partial B} S_{ijk}(P,Q)[u_k(Q) - u_k(P) - u_{k,m}(P)(y_m(Q) - y_m(P))] \, \mathrm{d}S_Q, \quad (34)$$

where the (strongly singular) kernel D_{ijk} and (hypersingular)

kernel S_{ijk} are:

$$D_{ijk} = \frac{1}{8\pi(1-\nu)r^2}[(1-2\nu)(\delta_{ki}r_{,j} + \delta_{kj}r_{,i} - \delta_{ij}r_{,k}) + 3r_{,i}r_{,j}r_{,k}], \tag{35}$$

$$S_{ijk} = \frac{G}{4\pi(1-\nu)r^3}\left[3\frac{\partial r}{\partial n}[(1-2\nu)\delta_{ij}r_{,k} + \nu(\delta_{ik}r_{,j} + \delta_{jk}r_{,i}) - 5r_{,i}r_{,j}r_{,k}]\right] + \frac{G}{4\pi(1-\nu)r^3}[3\nu(n_i r_{,j}r_{,k} + n_j r_{,i}r_{,k}) + (1-2\nu)(3n_k r_{,i}r_{,j} + n_j\delta_{ik} + n_i\delta_{jk}) - (1-4\nu)n_k\delta_{ij}]. \tag{36}$$

Again, taking the inner product of Eq. (34) with the source normal, one gets the equation:

$$0 = \int_{\partial B} D_{ijk}(P,Q)n_j(P)(\tau_k(Q) - \tau_k(P))\,\mathrm{d}S_Q - \sigma_{km}(P)\int_{\partial B} D_{ijk}(P,Q)n_j(P)(n_m(Q) - n_m(P))\,\mathrm{d}S_Q - \int_{\partial B} S_{ijk}(P,Q)n_j(P)[u_k(Q) - u_k(P) - u_{k,m}(P)(y_m(Q) - y_m(P))]\mathrm{d}S_Q. \tag{37}$$

The procedure for obtaining the displacement gradients $u_{k,m}$, that are required in Eqs. (34) and (37), is described in Appendix A. The stress components σ_{ij} can be easily obtained from the displacement gradients using Hooke's law.

6. Hypersingular boundary node method (HBNM)

Analogous to the development of the BNM in Section 4, derivation of the HBNM for potential theory and linear elasticity are presented in this Section. The goal here is to present a comprehensive treatment of the method.

6.1. Potential theory

Using the interpolation functions τ (second part of the Eq. (8)) and for the tangential derivatives of u (Eq. (19)), one can obtain the discretized forms of the potential gradient (see Eq. (33)) and the HBIEs Eqs. (31) and (32) as follows:

$$\nabla u = \sum_{I=1}^{n} \Psi_I^{(1)}\hat{u}_I\mathbf{t}_1 + \sum_{I=1}^{n} \Psi_I^{(2)}\hat{u}_I\mathbf{t}_2 + \sum_{I=1}^{n} \Phi_I\hat{\tau}_I\mathbf{n} \tag{38}$$

$$0 = \sum_{i=1}^{N_c}\int_{\partial B_i}\frac{\partial G(P,Q)}{\partial x_m(P)}\left[\sum_{I=1}^{N_Q}\Phi_I(Q)\hat{\tau}_I - \sum_{I=1}^{N_Q}\Phi_I(P)\hat{\tau}_I\right] - u_{,k}(P)\int_{\partial B_i}\frac{\partial G(P,Q)}{\partial x_m(P)}(n_k(Q) - n_k(P))\,\mathrm{d}S_Q - \int_{\partial B_i}\frac{\partial F(P,Q)}{\partial x_m(P)}\left[\sum_{I=1}^{N_Q}\Phi_I(Q)\hat{u}_I - \sum_{I=1}^{N_P}\Phi_I(P)\hat{u}_I - u_{,k}(P)\times(x_k(Q) - x_k(P))\right]\mathrm{d}S_Q, \tag{39}$$

$$0 = \sum_{i=1}^{N_c}\int_{\partial B_i}\frac{\partial G(P,Q)}{\partial n(P)}\left[\sum_{I=1}^{N_Q}\Phi_I(Q)\hat{\tau}_I - \sum_{I=1}^{N_P}\Phi_I(P)\hat{\tau}_I\right] - u_{,k}(P)\int_{\partial B_i}\frac{\partial G(P,Q)}{\partial n(P)}(n_k(Q) - n_k(P))\mathrm{d}S_Q - \int_{\partial B_i}\frac{\partial F(P,Q)}{\partial n(P)}\left[\sum_{I=1}^{N_Q}\Phi_I(Q)\hat{u}_I - \sum_{I=1}^{N_P}\Phi_I(P)\hat{u}_I - u_{,k}(P)\times(x_k(Q) - x_k(P))\right]\mathrm{d}S_Q, \tag{40}$$

respectively, where $\Phi_I(P)$ and $\Phi_I(Q)$ are the contributions from the Ith node to the collocation point P and field point Q, respectively, with N_P and N_Q nodes in their respective domains of dependence. Of course, the gradient of u from Eq. (38), in global coordinates, is used in Eqs. (39) and (40).

6.2. Linear elasticity

As mentioned before, the procedure for obtaining $u_{k,m}$ in the elasticity Eqs. (34) and (37), from the tangential derivatives and tractions, is described in Appendix A. Once this is done, discretized versions of Eqs. (34) and (37) are readily obtained as:

$$0 = \sum_{l=1}^{N_c}\int_{\partial B_l} D_{ijk}(P,Q)\left[\sum_{I=1}^{N_Q}\Phi_I(Q)\hat{\tau}_{kI} - \sum_{I=1}^{N_P}\Phi_I(P)\hat{\tau}_{KI}\right]\times\mathrm{d}S_Q - \sigma_{km}(P)\int_{\partial B_l} D_{ijk}(P,Q)(n_m(Q) - n_m(P))\,\mathrm{d}S_Q - \int_{\partial B_l} S_{ijk}(P,Q)\left[\sum_{I=1}^{N_Q}\Phi_I(Q)\hat{u}_{kI} - \sum_{I=1}^{N_P}\Phi_I(P)\hat{u}_{kI} - u_{k,m}(P)(y_m(Q) - y_m(P))\right]\mathrm{d}S_Q \tag{41}$$

and

$$0 = \sum_{l=1}^{N_c} \int_{\partial B_l} D_{ijk}(P,Q) n_j(P) \left[\sum_{I=1}^{N_Q} \Phi_I(Q) \hat{\tau}_{kI} - \sum_{I=1}^{N_P} \Phi_I(P) \hat{\tau}_{kI} \right] \times \mathrm{d}S_Q - \sigma_{km}(P) \int_{\partial B_l} D_{ijk}(P,Q) n_j(P) (n_m(Q) - n_m(P)) \, \mathrm{d}S_Q - \int_{\partial B_l} S_{ijk}(P,Q) n_j(P) \times \left[\sum_{I=1}^{N_Q} \Phi_I(Q) \hat{u}_{kI} - \sum_{I=1}^{N_P} \Phi_I(P) \hat{u}_{kI} - u_{k,m}(P)(y_m(Q) - y_m(P)) \right] \mathrm{d}S_Q. \quad (42)$$

6.3. Discretization

Eqs. (39) and (40) are the HBNM equations for potential theory, and Eqs. (41) and (42) are the HBNM equations for linear elasticity. In this work, Eq. (40) is used to solve boundary value problems (BVPs) in potential theory and Eq. (42) is used to solve BVPs in linear elasticity.

The procedure followed for discretization of Eqs. (40) and (42) is quite analogous to the BNM case described before in Section 4.3. These equations are fully regularized and contain either non-singular or weakly integrands. Non-singular integrals are evaluated using the usual Gauss quadrature over surface cells, while the weakly singular integrals are evaluated using the procedure outlined in Ref. [58,65]. The discretized version of either Eqs. (40) or (42) has the generic form shown in Eq. (30). Numerical results from the BNM, for 3-D potential theory and linear elasticity, are available in Refs. [58,59], respectively, while corresponding numerical results from the HBNM are presented in this paper.

7. Numerical results

The HBNM is used herein to solve BVPs in potential theory (Laplace's equation) and linear elasticity. The numerical examples presented provide considerable insight into the working of the method and choice of various parameters. Several aspects of the HBNM are investigated such as positioning of collocation nodes, determination of geodesics, range of influence of nodes (d_l), solution at internal points, accuracy, and convergence properties. Corresponding numerical results from the standard BNM have been given by Chati et al. [59] and Chati and Mukherjee [58]. The numerical results presented for the solution of BVPs using the HBNM not only validate the method itself, but also indicate its advantage for solving other problems for which HBIEs are of special importance (e.g. error analysis and adaptivity — please find a detailed discussion of this issue in Ref. [51]).

7.1. Potential theory — Dirichlet problems on a sphere

The Laplace's equation in 3-D can be written as:

$$\nabla^2 u = \frac{\partial^2 u}{\partial x_1^2} + \frac{\partial^2 u}{\partial x_2^2} + \frac{\partial^2 u}{\partial x_3^2} = 0. \quad (43)$$

The HBNM is used to solve Dirichlet problems on a sphere. The exact solutions presented below have been used to evaluate the performance of the various parameters of the HBNM. Dirichlet problems are posed with these solutions imposed (in turn) on the surface of a solid sphere, and the normal derivatives of the potential are computed on the sphere surface. Potential gradients at internal points are also computed in some cases. The complete sphere is modeled in all cases.

- Linear solution

$$u = x_1 + x_2 + x_3. \quad (44)$$

- Quadratic solution

$$u = x_1 x_2 + x_2 x_3 + x_3 x_1. \quad (45)$$

- Cubic solution

$$u = x_1^3 + x_2^3 + x_3^3 - 3x_1^2 x_2 - 3x_2^2 x_3 - 3x_3^2 x_1. \quad (46)$$

- Trigonometric solution

$$u = \frac{2r^2}{R^2} \cos^2 \phi - \frac{2r^2}{3R^2} - \frac{1}{3}, \quad (47)$$

where R is the radius of the sphere, ϕ is the angle measured from the x_3 axis and $r^2 = x_1^2 + x_2^2 + x_3^2$.

Positioning of collocation nodes. The location of the collocation node in each cell is an important ingredient for the successful implementation of the method. Table 1 presents the global L_2 error in $\partial u/\partial n$ (on the surface of the sphere) for the linear, quadratic and cubic solutions (imposed as Dirichlet boundary conditions on the sphere surface) for various positions of the single collocation node in the parent space (s, t). The global (L_2) error in a function is computed according to the equation;

$$\epsilon(\phi) = \frac{\int_A \left(\phi^{(\text{exact})} - \phi^{(\text{numerical})} \right)^2 \mathrm{d}A}{\int_A (\phi^{(\text{exact})})^2 \mathrm{d}A} 100\% \quad (48)$$

where ϕ is the variable of interest and A is either the area of a panel or of the whole surface ∂B.

The mapping of a triangular surface cell to the parent space (s,t) is shown in Fig. 3. The results have been obtained

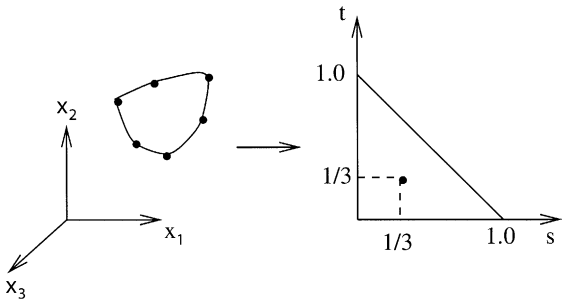

Fig. 3. Mapping of quadratic triangular cell (T6) to the parent space (s,t).

using a configuration consisting of 72 T6 triangles with one node per cell. It can be clearly seen from Table 1 that, as expected, placement of the collocation node at the centroid of the triangle in the parent space, i.e $s = t = 1/3$, yields excellent results. Overall, placing the single node at the centroid of the triangle/rectangle yields the best numerical results.

Geodesics. In order to construct the interpolating functions using MLS approximants, it is necessary to compute the geodesic on the bounding surface of a body. Computation of geodesics can get quite cumbersome on a general curved surface described by splines. For the sphere, the exact geodesic between two points P (collocation node) and Q (field point) is the length of the arc between these points on the great circle containing them. However, a very simple approximation to the geodesic would be to use the 'Euclidean' distance between points P and Q. Table 2 summarizes the procedure for computing the exact and approximate geodesic on a sphere, while Table 3 presents a comparison in the L_2 errors for linear, quadratic, cubic and trigonometric solutions imposed on the sphere. For this specific example, with idealized geometry and boundary conditions, it can be seen that the errors remain reasonably small even if the approximate geodesic is used to replace the exact one. Thus, it is expected that the computation of geodesics on complicated shapes will not be a hindrance towards using the present methodology.

Range of influence of nodes. Another important feature of the MLS approximants is the range of influence associated with each node. The parameter which controls the so called

Table 1
$\epsilon(\partial u/\partial n)$: L_2 error in $\partial u/\partial n$ (Eq. (48)) for Dirichlet problems on a sphere for various positions of the single collocation node in the parent space

$s = t$	Linear(%)	Quadratic (%)	Cubic (%)
0.1	4.369	8.735	30.264
0.15	3.692	5.982	23.405
0.2	0.519	2.404	11.414
0.25	0.336	1.271	5.628
0.3	0.185	0.730	3.625
1/3	0.0717	0.313	1.665
0.35	0.153	0.593	2.2187
0.4	0.454	1.111	2.566

Table 2
Exact versus approximate geodesics on the surface of a sphere

Collocation point	P $(x_{1P}, x_{2P}, x_{3P}) \equiv (R, \theta_P, \phi_P)$
Field point	Q $(x_{1Q}, x_{2Q}, x_{3Q}) \equiv (R, \theta_Q, \phi_Q)$
Curvilinear coordinates between P and Q	$\tilde{s}_1 = R(\phi_Q - \phi_P)$; $\tilde{s}_2 = R(\theta_Q - \theta_P)$
Exact geodesic	Approximate geodesic
Ψ: Angle between P and Q $\Psi = \arccos(\bar{r}_P \cdot \bar{r}_Q / R^2)$ $d = R\Psi$	$d = \sqrt{(\tilde{s}_1^2 + \tilde{s}_2^2)}$

'compact support' associated with each node is d_I. In this work the parameter d_I is chosen to be *non-homogeneous* in the sense that each evaluation point has an *identical* number of nodes in its domain of dependence. Now, for a given polynomial basis (e.g. Linear/Quadratic/Cubic), the number of nodes n in the domain of dependence of each evaluation point becomes the parameter of interest.

The parameters d_I are chosen as follows. For a given n, let S be the set of nodes in the domain of dependence of a particular evaluation point E. The values of d_I for all nodes in S are set equal to $d_{\max}$, where $d_{\max}$ is the distance from E, along the geodesic, of the node in S, which is farthest from E.

Fig. 4(a) and (b) show the effect of varying the number of nodes n for a linear basis ($m = 3$) and a quadratic basis ($m = 6$), respectively, for the cubic and trigonometric solutions. It is observed that the lowest value of L_2 errors is obtained for $n \in (2m,3m)$. This fact has also been observed for the BNM ([58]).

Potential and gradient at internal points. Fig. 5(a) and (b) show variation in the potential and its x_1 derivative, respectively, for points along the x_1 axis inside the sphere. The Dirichlet boundary value problem is solved upon imposing the trigonometric solution on a cell configuration consisting of 72 T6 cells with one node per cell and a quadratic basis ($m = 6$). It is seen from these figures that the HBNM solutions match the exact solutions within plotting accuracy for both u and $\partial u/\partial x_1$.

An important point needs to be made here. Some kernels in a BIE or HBIE become nearly singular when collocated at an internal point that is close to the boundary of a body. This can lead to large errors in a BNM or HBNM numerical solution at such points. This matter has been dealt with by several researchers. The reader is referred to a recent paper by Mukherjee et al. [66] for a detailed discussion of nearly

Table 3
$\epsilon(\partial u/\partial n)$: L_2 error in $\partial u/\partial n$ for Dirichlet problems on a sphere for the exact and an approximate computation of geodesics

Exact solution	Exact geodesic (%)	Approximate geodesic (%)
Linear	0.717	0.109
Quadratic	0.313	0.715
Cubic	1.665	4.059
Trigonometric	0.172	0.279

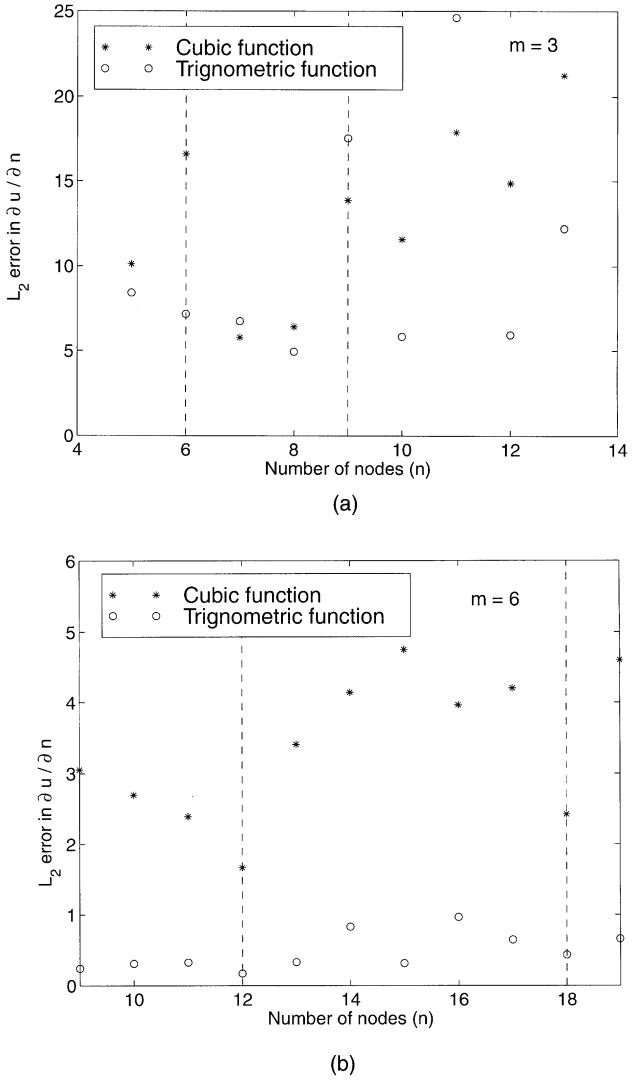

Fig. 4. $\epsilon(\partial u/\partial n)$: L_2 error in $\partial u/\partial n$ for varying number of points in the domain of dependence of an evaluation point E; (a) linear polynomial basis ($m = 3$); (b) quadratic polynomial basis ($m = 6$) (72 T6 cells with one node per cell).

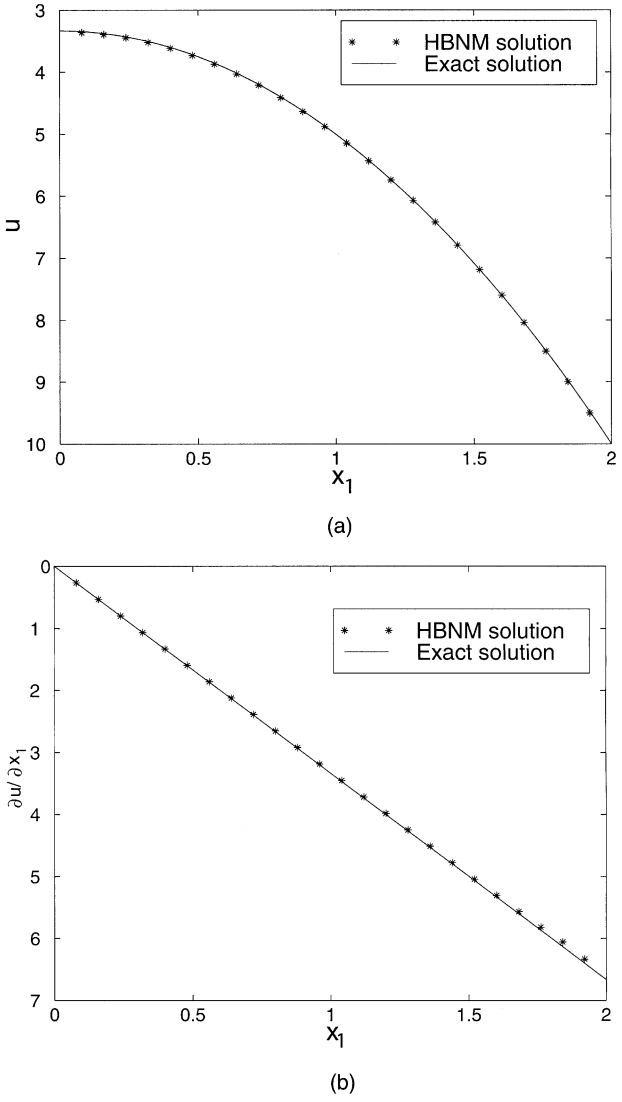

Fig. 5. Variation of (a) potential and (b) $\partial u/\partial x_1$ along the x_1 axis for a sphere with the trigonometric solution.

singular integrals in the context of the BNM and the HBNM. The approach presented in Ref. [66] has been employed in the present paper in order to obtain accurate values of u and $\partial u/\partial x_1$ (at internal points close to the surface of a body) in Fig. 5, as well as for obtaining the elasticity results presented in Section 7.2.

Convergence study. The results obtained by the HBNM have also been compared with those from the conventional BEM for a Dirichlet problem on a sphere with the trigonometric solution (Eq. (47)). Fig. 6 presents a comparison in the L_2 error in $\partial u/\partial n$ for the HBNM and BEM, as functions of the (global) number of nodes. The L_2 error $e(\phi)$ is defined here as:

$$e(\phi) = \log\{\|\phi^{(n)} - \phi^{(e)}\|/\|\phi^{(e)}\|\}, \tag{49}$$

where $\|\phi\| = \sum_{i=1}^{N} (\phi_i)^2$. Here, ϕ_i are the nodal values of the function ϕ and the superscripts n and e refer to its numerical and exact values, respectively. Also, as mentioned above, N is the total number of nodes on ∂B.

Fig. 6 shows that the two methods yield comparable results and have similar rates of convergence. The HBNM solution, however, is more accurate than the BEM solution for this example.

7.2. Linear elasticity

Two benchmark elasticity test problems are solved by the HBNM. These examples are the 3-D versions of the Lamé and Kirsch problems.

7.2.1. 3-D Lamé problem

The 3-D Lamé problem consists of a hollow sphere, with inner and outer radius a and b, respectively, under internal

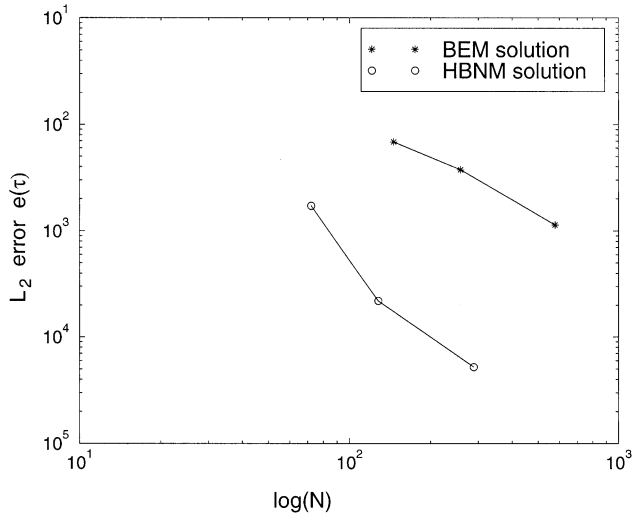

Fig. 6. Comparison of $e(\tau)$ (L_2 error in $\partial u/\partial n$) for the HBNM and the conventional BEM for a Dirichlet problem on a sphere. N is the total number of nodes (one node per cell is used in the HBNM).

pressure. Fig. 7 shows a schematic of the problem under consideration. The numerical solution for this problem has been obtained using the material parameters $E = 1.0$, $\nu = 0.25$, and geometric parameters $a = 1.0$, $b = 4.0$ with internal pressure $p_i = 1$. The numerical solution has been obtained by prescribing tractions all over the boundary and then modifying the resulting singular matrix using the ideas presented in the paper by Lutz et al. [67] and Chati et al. [59].

The entire surface of the hollow sphere has been modeled here, i.e. symmetry conditions have not been used. The exact solution for the radial displacement, radial and tangential stresses, as functions of the distance r from the center of the sphere, is given as ([68]):

$$u_r = \frac{p_i a^3 r}{E(b^3 - a^3)}\left[(1 - 2\nu) + (1 + \nu)\frac{b^3}{2r^3}\right], \tag{50}$$

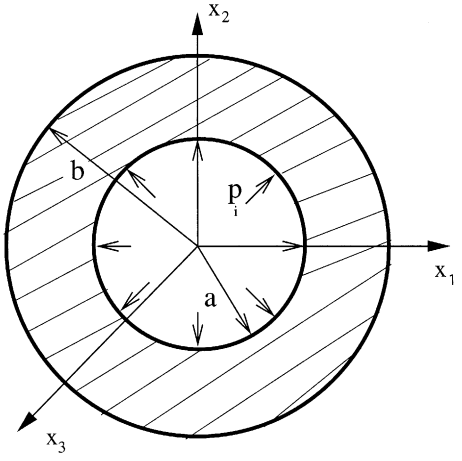

Fig. 7. Lamé problem for a hollow sphere under internal pressure.

$$\sigma_{rr} = \frac{p_i a^3 (b^3 - r^3)}{r^3 (a^3 - b^3)}, \tag{51}$$

$$\sigma_{tt} = \frac{p_i a^3 (2r^3 + b^3)}{2r^3 (b^3 - a^3)}. \tag{52}$$

The cell/nodal structure used to obtain the numerical results consists of 72 quadratic T6 cells on each surface of the hollow sphere with 1 node per cell.

Fig. 8(a) shows the radial displacement along the x_1-axis compared with the analytical solution. The radial and tangential stresses are compared to the exact solution in Fig. 8(b). It can be clearly seen that the numerical results are in excellent agreement with the analytical solution. The algorithm presented in Mukherjee et al. [66] is crucial for obtaining accurate solutions for the displacement and stresses at internal points close to the boundary. Also, a

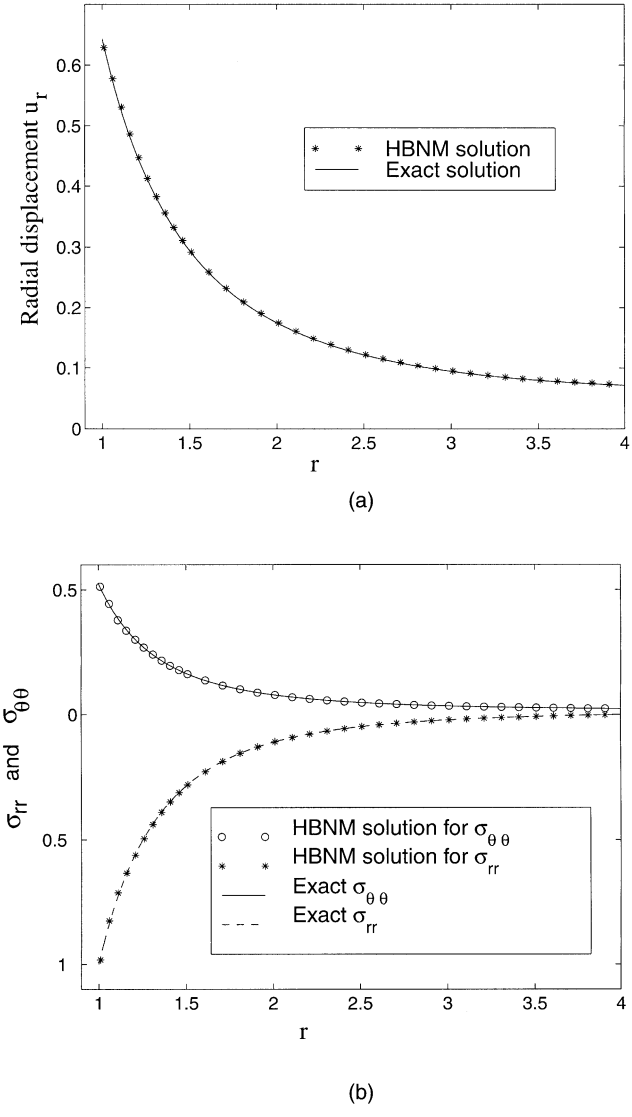

Fig. 8. Internal (a) radial displacement and (b) radial and tangential stresses, along the x_1 axis for the Lamé problem.

Table 4
Convergence study for $\in u_r$) the L_2 error in radial displacement (u_r), on the inner and outer surfaces of the sphere, for the 3-D Lamé problem

L_2 error	144 cells (%)	256 cells (%)	576 cells (%)
Outer surface	0.404	0.241	0.0496
Inner surface	0.460	0.214	0.0658

convergence study is carried out to demonstrate the robustness of the proposed numerical method. Table 4 shows the L_2 error in the radial displacement (u_r) on the inner and outer surfaces of the sphere. One node per cell is used in all the calculations. As the number of cell increases, the L_2 error decreases on both the outer and inner surfaces of the sphere for the 3-D Lamé problem.

7.2.2. 3-D Kirsch problem

The 3-D Kirsch problem consists of examining the stress distribution in the vicinity of a small spherical cavity in a cube subjected to far field uniform tension, as illustrated in Fig. 9. The material parameters are chosen to be: $E = 1.0$, $\nu = 0.25$. The geometric parameters are chosen as: $a = 1.0$, $b = 10.0$. Again, the loading is applied without restraining any rigid body modes and the scheme by Chati et al. [59] is used to obtain meaningful numerical results.

The exact solution for the normal stress (σ_{33}), for points in the plane $x_3 = 0$, is given as (Timoshenko and Goodier [68]):

$$\sigma_{33} = \sigma_0\left[1 + \frac{4-5\nu}{2(7-5\nu)}\left(\frac{a}{r}\right)^3 + \frac{9}{2(7-5\nu)}\left(\frac{a}{r}\right)^5\right]. \quad (53)$$

Here r is the distance of a generic point from the center of the spherical cavity.

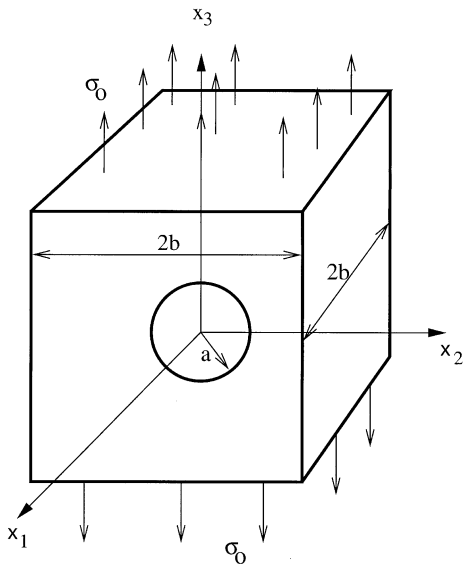

Fig. 9. 3-D Kirsch problem: a cube with a spherical cavity loaded in far-field uniaxial tension

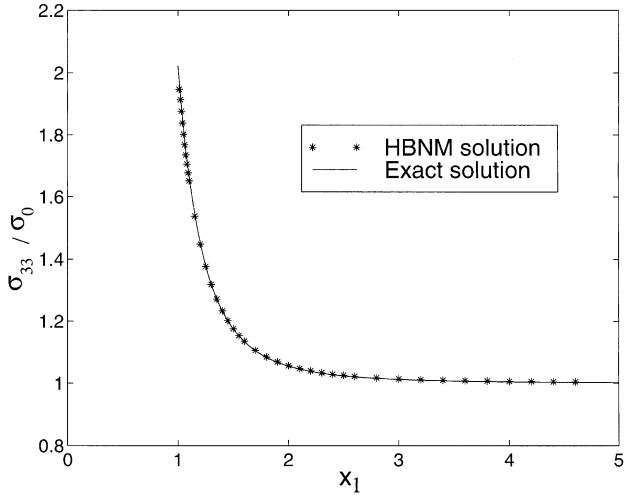

Fig. 10. σ_{33} along the x_1 axis ahead of the cavity for the Kirsch problem.

Fig. 10 shows a comparison between the HBNM solution and the exact solution for the normal stress (σ_{33}) along the x_1 axis. It can be clearly seen that the HBNM solution is in excellent agreement with the analytical solution. The cell structure consists of 96 Q4 cells modeling the cube and 72 T6 cells modeling the spherical cavity, again with one node per cell. It is again pointed out that the new algorithm mentioned in Ref. [66] is essential for obtaining accurate values of stresses near the surface of the cavity.

8. Concluding remarks

A new meshfree method called the HBNM, that combines HBIEs with MLS approximants, has been presented in this paper. The efficacy of the HBNM is demonstrated by comparing numerical results, for several 3-D numerical examples in potential theory and in linear elasticity, with analytical solutions for these problems. The HBNM, presented here, is expected to be very useful for obtaining meshfree formulations of diverse important problems such as 3-D fracture mechanics, error analysis and adaptivity and Symmetric Galerkin Boundary Element Methods. Work on error analysis and adaptivity is already in progress [51], while work on the other topics, mentioned above, is planned for the near future.

Acknowledgements

The Cornell group (Chati and Mukherjee) acknowledges support by the University Research Programs (URP) grant from Ford Motor Company to Cornell University. Professor Paulino acknowledges support from the National Science Foundation under Grant CMS-9713008. The computing for this research was carried out using the resources of the Cornell Theory Center, which receives funding from Cornell University, New York State, the National Center

for Research Resources at the National Institutes of Health, the National Science Foundation, the Defense Department Modernization program, the United States Department of Agriculture, and corporate partners. The efforts of Prachi Chati for carefully proof reading the manuscript are acknowledged.

Appendix A. Displacement gradient on the surface

The displacement gradient at a boundary source point P is needed in order to solve a boundary value problem in linear elasticity using the HBNM (see Eqs. (41) and (42)). Lutz et al. [39] have proposed a scheme for doing this, however, details of the procedure have not been provided in Ref. [39]. These details are given below.

The (right-handed) global Cartesian coordinates, as before, are (x_1, x_2, x_3). Consider (right-handed) local Cartesian coordinates (x_1', x_2', x_3') at a regular point P on ∂B as shown in Fig. 11. The local coordinate system is oriented such that the x_1' and x_2' coordinates lie along the tangential unit vectors $\mathbf{t}_1$ and $\mathbf{t}_2$ while x_3' is measured along the outward normal unit vector $\mathbf{n}$ to ∂B as defined in Eq. (33).

Therefore, one has:

$$\mathbf{x}' = \mathbf{Q}\mathbf{x}, \tag{A1}$$

$$\mathbf{u}' = \mathbf{Q}\mathbf{u}, \tag{A2}$$

where u_k', $k = 1, 2, 3$ are the components of the displacement vector $\mathbf{u}$ in the local coordinate frame, and the orthogonal transformation matrix $\mathbf{Q}$ has the components:

$$\mathbf{Q} = \begin{bmatrix} t_{11} & t_{12} & t_{13} \\ t_{21} & t_{22} & t_{23} \\ n_1 & n_2 & n_3 \end{bmatrix} \tag{A3}$$

with t_{ij} the jth component of the ith tangent vector and (n_1,n_2,n_3) the components of the normal vector.

The tangential derivatives of the displacement, in local coordinates, are $u_{i,k'}'$, $i = 1, 2, 3$; $k = 1, 2$. These quantities

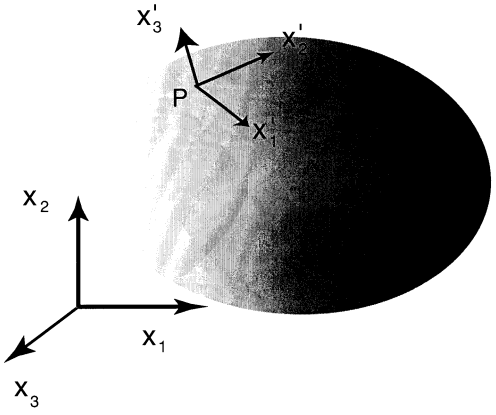

Fig. 11. Local coordinate system on the surface of a body.

are obtained as follows:

$$u_{i,k'}' \equiv \frac{\partial u_i'}{\partial s_k} = \mathrm{Q}_{ij}\frac{\partial u_j}{\partial s_k} = \mathrm{Q}_{ij}\sum_{I=1}^{n} \Psi_I^{(k)} \hat{u}_{j\mathrm{I}} \tag{A4}$$

where the last equality is obtained from Eq. (19).

The remaining components of $\nabla\mathbf{u}$ in local coordinates are obtained from Hooke's law (see [39]) as:

$$\frac{\partial u_1'}{\partial x_3'} = \frac{\tau_1'}{G} - \frac{\partial u_3'}{\partial x_1'}$$

$$\frac{\partial u_2'}{\partial x_3'} = \frac{\tau_2'}{G} - \frac{\partial u_3'}{\partial x_2'}$$

$$\frac{\partial u_3'}{\partial x_3'} = \frac{(1-2\nu)\tau_3'}{2G(1-\nu)} - \frac{\nu}{1-\nu}\left[\frac{\partial u_1'}{\partial x_1'} + \frac{\partial u_2'}{\partial x_2'}\right], \tag{A5}$$

where τ_k', $k = 1, 2, 3$, are the components of the traction vector in local coordinates.

The components of the displacement gradient tensor, in the local coordinate system, are now known. They can be written as:

$$(\nabla\mathbf{u})_{\mathrm{local}} \equiv \mathbf{A}' = \begin{bmatrix} u_{1,1'}' & u_{1,2'}' & u_{1,3'}' \\ u_{2,1'}' & u_{2,2'}' & u_{2,3'}' \\ u_{3,1'}' & u_{3,2'}' & u_{3,3'}' \end{bmatrix} \tag{A6}$$

Finally, the components of $\nabla\mathbf{u}$ in the global coordinate frame are obtained from those in the local coordinate frame by using the tensor transformation rule:

$$(\nabla\mathbf{u})_{\mathrm{global}} \equiv \mathbf{A} = \mathbf{Q}^T\mathbf{A}'\mathbf{Q} = \begin{bmatrix} u_{1,1} & u_{1,2} & u_{1,3} \\ u_{2,1} & u_{2,2} & u_{2,3} \\ u_{3,1} & u_{3,2} & u_{3,3} \end{bmatrix}. \tag{A7}$$

The gradient of the displacement field in global coordinates is now ready for use in Eq. (42).

References

[1] Mackerle J. Mesh generation and refinement for FEM and BEM — a bibliography (1990–1993). Finite Elem Anal Des 1993:177–88.
[2] Nayroles B, Touzot G, Villon P. Generalizing the finite element method: diffuse approximation and diffuse elements. Comput Mech 1992;10:307–18.
[3] Belytschko T, Lu YY, Gu L. Element-free Galerkin methods. Int J Numer Meth Engng 1994;37:229–56.
[4] Liu WK, Jun S, Zhang Y. Reproducing kernel particle methods. Inter J Numer Meth Fluids 1995;20:1081–106.
[5] Duarte CAM, Oden JT. H-p clouds — an h–p meshless method. Numer Meth Partial Differential Equations 1996;12:673–705.
[6] Duarte CAM, Oden JT. An h-p adaptive method using clouds. Comput Meth Appl Mech Engng 1996;139:237–62.
[7] Oden JT, Duarte CAM, Zienkiewicz OC. A new cloud-based hp finite element method. Comput Meth Appl Mech Engng 1998;153:117–26.
[8] Atluri SN, Zhu T. New meshless local Petrov-Galerkin (MPLG) approach in computational mechanics. Comput Mech 1998;22:117–27.

[9] Atluri SN, Zhu T. A new meshless local Petrov-Galerkin (MPLG) approach to nonlinear problems in computer modeling and simulation. Comput Modelling Simulation Engng 1998;3:187–96.
[10] Zhu T, Zhang J-D, Atluri SN. A local boundary integral equation (LBIE) method in computational mechanics, and a meshless discretization approach. Comput Mech 1998;21:223–35.
[11] Sukumar N, Moran B, Belytschko T. The natural element method. Int J Numer Mech Engng 1998;43:839–87.
[12] Strouboulis T, Babuška I, Copps K. The design and analysis of the Generalized Finite Element Method. Comput Meth Appl Mech Engng 2000;181:43–69.
[13] Moës N, Dolbow J, Belytschko T. A finite element method for crack growth without remeshing. Int J Numer Methods Engng 1999;46:131–50.
[14] Barry W, Saigal S. A three-dimensional element-free Galerkin elastic and elastoplastic formulation. Int J Numer Methods Engng 1999;46:671–93.
[15] Sukumar N, Moran B, Black T, Belytschko T. An element-free Galerkin method for three-dimensional fracture mechanics. Comput Mech 1997;20:170–5.
[16] Belytschko T, Lu YY, Gu L. Crack propagation by element-free Galerkin methods. Engng Fracture Mech 1995;51:295–315.
[17] Xu Y, Saigal S. An element-free Galerkin formulation for stable crack growth in elastic solids. Comput Methods Appl Mech Engng 1998;154:331–43.
[18] Krysl P, Belytschko T. The element free Galerkin method for dynamic propagation of arbitrary 3-D cracks. Int J Numer Methods Engng 1999;44:767–800.
[19] Belytschko T, Lu YY, Gu L, Tabbara M. Element-free Galerkin methods for static and dynamic fracture. Int J Solids Struct 1995;32:2547–70.
[20] Belytschko T, Tabbara M. Dynamic fracture using element-free Galerkin methods. Int J Numer Methods Engng 1996;39:923–38.
[21] Xu Y, Saigal S. Element-free Galerkin study of steady quasi-static crack growth in plane strain tension in elastic-plastic materials. Comput Mech 1998;21:276–82.
[22] Xu Y, Saigal S. An element-free Galerkin analysis of steady dynamic growth of a mode I crack in elastic-plastic materials. Int J Solids Struct 1999;36:1045–79.
[23] Krysl P, Belytschko T. Analysis of thin plates by the element-free Galerkin method. Comput Mech 1995;17:26–35.
[24] Krysl P, Belytschko T. Analysis of thin shells by the element-free Galerkin method. Int J Solids Struct 1996;33:3057–80.
[25] Bobaru F, Mukherjee S. Shape sensitivity analysis and shape optimization planar elasticity using the element-free Galerkin method. Comput Meth Appl Mech Engng 2001;190:4317–37.
[26] Belytschko T, Krongauz Y, Organ D, Fleming M, Krysl P. Meshless methods: an overview and recent developments. Comput Meth Appl Mech Engng 1996;139:3–47.
[27] Liu WK, Chen Y, Uras RA, Chang CT. Generalized multiple scale reproducing kernel particle methods. Comput Methods Appl Mech Engng 1996;139:91–157.
[28] Liu WK, Chen Y, Jun S, Belytschko T, Pan C, Uras RA, Chang CT. Overview and applications of the reproducing kernel particle methods. Arch Comput Methods Engng 1996;3:3–80.
[29] Krishnasamy G, Rizzo FJ, Rudolphi TJ. Hypersingular boundary integral equations: their occurrence, interpretation, regularization and computation. In: Banerjee PK, Kobayashi S, editors. Developments in Boundary Element Methods, 7. London: Elsevier, 1992. p. 207–52.
[30] Tanaka MV, Sladek V, Sladek J. Regularization techniques applied to boundary element methods. ASME Appl Mech Rev 1994;47:457–99.
[31] Paulino GH. Novel formulations of the boundary element method for fracture mechanics and error estimation. PhD. Dissertation, Cornell University, Ithaca, NY, 1995.
[32] Chen JT, Hong H-K. Review of dual boundary element methods with emphasis on hypersingular integrals and divergent series. ASME Appl Mech Rev 1999;52:17–33.
[33] Guiggiani M. Hypersingular formulation for boundary stress evaluation. Engng Anal Boundary Elem 1994;13:169–79.
[34] Wilde AJ, Aliabadi MH. Direct evaluation of boundary stresses in the 3-D BEM of elastostatics. Commun Numer Methods Engng 1998;14:505–17.
[35] Zhao ZY, Lan SR. Boundary stress calculation — A comparison study. Comput Struct 1999;71:77–85.
[36] Chati MK, Mukherjee S. Evaluation of gradients on the boundary using fully regularized hypersingular boundary integral equations. Acta Mech 1999;135:41–45.
[37] Krishnasamy G, Schmerr LW, Rudolphi TJ, Rizzo FJ. Hypersingular boundary integral equations: some applications in acoustics and elastic wave scattering. ASME, J Appl Mech 1990;57:404–14.
[38] Gray LJ, Martha LF, Ingraffea AR. Hypersingular integrals in boundary element fracture analysis. Int J Numer Methods Engng 1990;29:1135–58.
[39] Lutz ED, Ingraffea AR, Gray LJ. Use of simple solutions for boundary integral methods in elasticity and fracture analysis. Int J Numer Methods Engng 1992;35:1737–51.
[40] Gray LJ, Paulino GH. Crack tip interpolation, revisited. SIAM J Appl Math 1998;58:428–55.
[41] Chan Y-S, Fannjiang AC, Paulino G.H. Integral equations with hypersingular kerneals — Theory and applications to fracture mechanics. (submitted for publication).
[42] Bonnet M. Regularized direct and indirect symmetric variational BIE formulations for three-dimensional elasticity. Engng Anal Boundary Elem 1995;15:93–102.
[43] Gray LJ, Balakrishna C, Kane JH. Symmetric Galerkin fracture analysis. Engng Anal Boundary Elem 1995;15:103–9.
[44] Gray LJ, Paulino GH. Symmetric Galerkin boundary integral fracture analysis for plane orthotropic elasticity. Comput Mech 1997;20:26–33.
[45] Gray LJ, Paulino GH. Symmetric Galerkin boundary integral formulation for interface and multizone problems. Int J Numer Methods Engng 1997;40:3085–101.
[46] Phan A-V, Mukherjee S, Mayer JRR. The hypersingular boundary contour method for two-dimensional linear elasticity. Acta Mech 1998;130:209–25.
[47] Mukherjee S, Mukherjee YX. The hypersingular boundary contour method for three-dimensional linear elasticity. ASME J Appl Mech 1998;65:300–9.
[48] Paulino GH, Gray LJ, Zarikian V. Hypersingular residuals — A new approach for error estimation in the boundary element method. Int J Numer Methods Engng 1996;39:2005–29.
[49] Menon G. Hypersingular error estimates in boundary element methods. M.S. Thesis, Cornell University, Ithaca, NY 1996.
[50] Menon G, Paulino GH, Mukherjee S. Analysis of hypersingular residual error estimates in boundary element methods for potential problems. Comput Methods Appl Mech Engng 1999;173:449–73.
[51] Chati MK, Paulino GH, Mukherjee S. The meshless standard and hypersingular boundary node methods — Applications to error estimation and adaptivity in three-dimensional problems. Int J Numer Methods Engng 2001;50:2233–69.
[52] Mukherjee YX, Mukherjee S. Error analysis and adaptivity in three-dimensional linear elasticity by the usual and hypersingular boundary contour methods. Int J Solids Struct 2001;38:161–78.
[53] Martin PA, Rizzo FJ. Hypersingular integrals: how smooth must the density be? Int J for Numer Methods Engng 1996;39:687–704.
[54] Cruse TA, Richardson JD. Non-singular Somigliana stress identities in elasticity. Int J Numer Methods Engng 1996;39:3273–304.
[55] Martin PA, Rizzo FJ, Cruse TA. Smoothness-relaxation strategies for singular and hypersingular integral equations. Int J Numer Methods Engng 1998;42:885–906.
[56] Mukherjee YX, Mukherjee S. The boundary node method for potential problems. Int J Numer Methods Engng 1997;40:797–815.
[57] Kothnur VS, Mukherjee S, Mukherjee YX. Two dimensional linear

elasticity by the boundary node method. Int J Solids Struct 1999;36:1129–47.
[58] Chati MK, Mukherjee S. The boundary node method for three-dimensional problems in potential theory. Int J Numer Methods Engng 2000;47:1523–47.
[59] Chati MK, Mukherjee S, Mukherjee YX. The boundary node method for three-dimensional linear elasticity. Int J Numer Methods Engng 1999;46:1163–84.
[60] Chati MK. Meshless standard and hypersingular boundary node method — Applications in three-dimensional potential theory and linear elasticity. PhD. Dissertation, Cornell University, Ithaca, NY, 1999.
[61] Banerjee PK. The Boundary Element Methods in Engineering. 2nd ed. New York: McGraw Hill, 1994.
[62] Rizzo FJ. An integral equation approach to boundary value problems of classical elastostatics. Quart Appl Math 1967;25:83–95.
[63] Zienkiwicz OC. The Finite Element Method. 3rd ed. New York: McGraw Hill, 1977.
[64] Bathe KJ. Finite Element Procedures in Engineering Analysis. Englewood Cliffs, NJ: Prentice-Hall, 1976.
[65] Nagarajan A, Mukherjee S. A mapping method for numerical evaluation of two-dimensional integrals with 1/r singularity. Comput Mech 1993;12:19–26.
[66] Mukherjee S, Chati MK, Shi X. Evaluation of nearly singular integrals in boundary element, contour and node methods for three-dimensional linear elasticity. Int J Solids Struct 2000;37:7633–54.
[67] Lutz ED, Ye W, Mukherjee S. Elimination of rigid body modes from discretized boundary integral equations. Int J Solids Struct 1998;35:4427–36.
[68] Timoshenko SP, Goodier JN. Theory of Elasticity. 3rd. ed. New York: McGraw Hill, 1976.